Center of mass states render multi-joint torques throughout standing balance recovery

Kristen L. Jakubowski[1 *]

Giovanni Martino[2]

Owen N. Beck[3]

Gregory S. Sawicki[4-7]

Lena H. Ting[1,8]

[1]Wallace H. Coulter Department of Biomedical Engineering, Emory University and Georgia Institute of Technology, Atlanta, GA, USA

[2]Department of Biomedical Sciences, University of Padova, Padua, Italy

[3]Department of Kinesiology and Health Education, University of Texas at Austin, Austin, TX, USA

[4]George W. Woodruff School of Mechanical Engineering, Georgia Institute of Technology, Atlanta, GA, USA

[5]Insitute for Robotics and Intelligent Machines, Georgia Institute of Technology, Atlanta, GA, USA

[6]School of Biological Sciences, Georgia Institute of Technology, Atlanta, GA, USA

[7]Institute for Human Machine Cognition, Pensacola, FL, USA

[8]Department of Rehabilitation Medicine, Division of Physical Therapy, Emory University, Atlanta, GA, USA

* Corresponding author

Kristen L. Jakubowski

kjakubo@emory.edu

RUNNING TITLE:

Center of mass states accurately predict joint torques

ABSTRACT

Successful reactive balance control requires coordinated modulation of hip, knee, and ankle torques. Stabilizing joint torques arise from neurally-mediated feedforward tonic muscle activation that modulates muscle short-range stiffness, which provides an instantaneous "mechanical feedback" to the perturbation. In contrast, neural feedback pathways activate muscles in response to sensory input, generating joint torques after a delay. However, the specific contributions from feedforward and feedback pathways to the balance-correcting torque response are poorly understood. Since feedforward- and feedback-mediated torque responses to balance perturbations act at different delays, we modified the sensorimotor response model (SRM), previously used to analyze the muscle activation response, to reconstruct joint torques using parallel feedback loops. Each loop is driven by the same information, center of mass (CoM) kinematics, but each loop has an independent delay. We evaluated whether a torque-SRM could decompose the reactive torques during balance-correcting responses to backward support surface translations at four magnitudes into the instantaneous "mechanical feedback" torque modulated by feedforward neural commands prior to the perturbation, and neurally-delayed feedback components. The SRM accurately reconstructed torques at the hip, knee, and ankle, across all perturbation magnitudes (R^2>0.84 & VAF>0.83). Moreover, the hip and knee exhibited feedforward and feedback components, while the ankle only exhibited feedback components. The lack of a feedforward component at the ankle may occur because the compliance of the Achilles tendon attenuates muscle short-range stiffness. Our model may provide a framework for evaluating changes in the feedforward and feedback contributions to balance that occur due to aging, injury, or disease.

KEYWORDS

motor control, sensorimotor feedback, feedforward control, tendon stiffness, postural control

NEWS AND NOTEWORTHY

Reactive balance control requires coordination of neurally-mediated feedforward and feedback pathways to generate stabilizing joint torques at the hip, knee, and ankle. Using a sensorimotor response model, we decomposed reactive joint torques into feedforward and feedback contributions based on delays relative to center of mass kinematics. Responses across joints were driven by the same signals, but contributions from feedforward versus feedback pathways

differed, likely due to differences in musculotendon properties between proximal and distal muscles.

INTRODUCTION

When responding to postural perturbations during standing, individuals rapidly produce corrective torques that are coordinated across the hip, knee, and ankle, arising from both feedforward and feedback pathways (Fig 1) (1, 2). The fastest the nervous system can generate a corrective torque through neurally-mediated sensory feedback pathways is approximately 100 ms—which includes both the conduction time and the neuromechanical delay (3, 4). During this delay, there is an instantaneous "mechanical feedback" torque that arises from the mechanical properties of activated muscle: muscle short-range stiffness that is tuned by anticipatory feedforward muscle activation (5, 6). We note that within this context, the neurally-mediated feedforward and feedback components within the joint torque response are both a reaction to the perturbation. While both feedforward and feedback components interact to stabilize the body following a postural perturbation (1, 2), differentiating the feedforward and feedback contributions to the overall reactive joint torque response remains an open challenge. Separately identifying the feedforward and feedback contributions would further the fundamental understanding of balance control and may also help identify specific mechanisms underlying balance impairments in older adults or individuals with neuromuscular diseases or injuries for the development of targeted rehabilitation. By leveraging knowledge about the delays associated with feedforward and feedback control, here, we sought to identify the feedforward and feedback contributions to balance-correcting joint torque responses at the hip, knee, and ankle during perturbations to standing balance.

Neurally-mediated feedforward tonic muscle activation gives rise to the background joint torque prior to the perturbation. Additionally, this background muscle activity modulates muscle short-range stiffness, which provides an instantaneous "mechanical feedback" torque to perturbations that cannot be mediated by sensorimotor feedback (7, 8). As such, we consider the neurally-mediated feedforward component as the instantaneous "mechanical feedback" torque to perturbations (e.g., the *neural feedforward* contribution alters a *mechanical feedback* component). Specifically, muscle short-range stiffness provides an instantaneous resistance to changes in muscle length and, thus, changes in joint angle, and the torque arising from muscle short-range stiffness reflects the mechanical properties of the muscle due to both its activation and movement history (5, 6, 9, 10). The nervous system can improve balance in uncertain environments by increasing the torque produced by muscle short-range stiffness in two ways:

feedforward increases in background muscle activation and co-contraction (11). Feedforward increases in muscle activation improve stability by increasing the torque produced by muscle short-range stiffness at the onset of the perturbation as muscle short-range stiffness scales linearly with the background force (6, 12). Co-contraction increases the short-range stiffness of multiple muscles spanning the joint, further increasing the resistance to unexpected perturbations (13). Modeling studies suggest that the nervous system may leverage feedforward muscle co-contraction during postural control in the presence of noise as a means to minimize the energetic cost compared to solely relying on feedback control. Additionally, individuals increase feedforward muscle co-contraction to increase postural stiffness when balance is challenged or threatened (14-18). However, feedforward strategies alone are insufficient to stabilize the body; thus, feedback control is also required to maintain postural stability (19-21).

Feedback responses are generated through sensorimotor transformations, where the nervous system receives sensory information (e.g., a sensory error) and translates it into reactive muscle activations that generate joint torque. Within this paper, we consider the neurally-mediated feedback component as the delayed reactive joint torques. The delay between the onset of a perturbation (e.g., the change in sensory feedback) to the onset of joint torque depends upon the sensory feedback pathway (e.g., subcortical or cortical pathways; Fig 1) and the neuromechanical delay—the latency between neural drive and muscle force production. We previously demonstrated that an error-based sensorimotor transformation of the delayed center of mass (CoM) kinematics (e.g., acceleration, velocity, and displacement) robustly explains reactive muscle activations (22). The sensorimotor response model (SRM) is based on the principle that the neuromuscular system coordinates the activation of muscles across the body to maintain task-level goals, such that coordinated muscle activations reflect task-relevant errors (e.g., CoM displacement) as opposed to joint-level errors (23). We have extensively used the SRM to predict feedback muscle activations across multiple joints and different perturbation conditions (22-26). Most recently, the EMG-SRM, through the implementation of parallel loops with independent parameters, has dissociated components of the long-latency ankle muscle response from subcortical versus cortical pathways (27). However, muscle intrinsic torque responses that arise due to neurally mediated feedforward activation are not accounted for in the EMG response to a perturbation, or the EMG-SRM.

It has previously been demonstrated that the same physiological principle that underlies the muscle activation response (the EMG-SRM) also underlies the torque response at the ankle (28). Afschrift, et al. (28) recently used a modified version of the SRM to estimate the sensorimotor feedback torque response about the ankle during balance recovery during standing and walking. Thus, it is feasible to use the torque-SRM to predict the multi-joint torque response. However, it is unclear whether a torque-SRM can predict the response at the hip and knee because prior modeling work suggests that the hip and knee both exhibit a feedforward muscle short-range stiffness response while the ankle does not (29). A torque-SRM may be unable to capture the feedforward muscle short-range stiffness response for two reasons. First, the SRM is a feedback model; thus, it may poorly predict the feedforward, short-range stiffness component in the torque response. While feedforward changes in muscle activation modulate the short-range stiffness response, we may be able to capture the short-range stiffness response within the torque-SRM since the short-range stiffness biomechanically appears as an instantaneous response to the perturbation (e.g., an instantaneous "mechanical feedback") (2, 5, 30). Second, the SRM model is driven by global CoM error, while a local stretch within the muscle drives the muscle short-range stiffness response. Thus, for a CoM-driven model to capture this joint-level response, the acceleration of the CoM would have to be strongly correlated to the angular acceleration of the joint, and it is unclear if that is the case during standing balance perturbations.

The aim of this study was to evaluate whether a delayed CoM-feedback model could accurately predict the entire time course of the multi-joint torque response to backward support-surface translations during standing. We hypothesized that CoM kinematics (acceleration, velocity, displacement) modulate the multi-joint reactive torque response to postural perturbations, with the fits being the best at the ankle. Second, we evaluated if the torque-SRM could differentiate the feedforward and feedback contributions to the torque response at each joint. To test our hypothesis, we examined the reactive torque response at the hip, knee, and ankle to backward support surface perturbations at four different magnitudes. We used the previously developed multi-loop EMG-SRM as the framework for our novel torque-SRM (27). More specifically, the new CoM-driven torque-SRM consisted of four parallel loops, so the input (CoM kinematics) and output (joint torque) of each loop were the same, but each loop had independent gains and delays (See *Sensorimotor Response Model (SRM)*). We demonstrate the utility of a CoM-feedback model for predicting the balance-correcting torque response at the hip,

knee, and ankle, and its ability to identify the feedforward and feedback mechanisms contributions to the overall response.

MATERIALS AND METHODS

Participants

Eight healthy young adults (4 females and 4 males; age 25 ± 4 years; height 1.74 ± 0.08 m; mass 71 ± 8 kg) participated in this study. All participants reported no history of neurological or musculoskeletal disorders. The Emory Institutional Review Board approved the study, and all methods were carried out according to the approved protocol (IRB00082414).

Data collection

This work is part of a larger study, and a portion of the data presented here has previously been published (20). Participants were instructed to maintain balance during ramp-and-hold support surface translations while standing on a custom platform (Factory Automation Systems, Atlanta, GA). Participants stood on two independent force plates embedded in the platform (AMTI, Watertown, MA, USA). Ground reaction forces were collected at 1000 Hz. Participants were instructed to stand with their bare feet 22 cm apart, with their weight evenly distributed between both feet and their arms crossed about their torso. Participants wore a 33-marker set based on a modified version of the Vicon Plug-in Gait model (31) that included additional foot markers (fifth metatarsal, medial and lateral heel, and medial malleolus).

Surface electromyography (EMG) data were collected at 1000 Hz from the medial gastrocnemius, soleus, tibialis anterior, rectus femoris, vastus medialis, biceps femoris, and gluteus medius on the left leg (Motion Lab Systems, Inc., Baton Rouge, LA, USA). Standard skin preparation methods were performed prior to electrode placement (32), and electrodes were placed on the belly of the muscle. Electromyography (EMG) signals were amplified to maximize the signal resolution in each channel. All kinetic and EMG data were synchronized with kinematic data (collected at 100 Hz) using a motion capture system (Vicon, UK, Oxford).

To identify a set of increasingly challenging perturbations for each individual, we first quantified balance capacity by determining each participant's step threshold to backward support surface translations (i.e., the platform moved the participant's feet posteriorly). Step threshold was defined as the maximum translation magnitude where participants could maintain balance

without taking a corrective step or being caught by the safety harness (20, 33-35). We used an adaptive method running fit (AMRF) algorithm from the Palamedes toolbox (36), which progressively increased (if no step was taken) or decreased (if a step was taken) the magnitude of the platform translation starting at 15cm. For each perturbation, platform acceleration and velocity were scaled with displacement such that braking occurred ~500 ms after perturbation onset. Catch trials (e.g., forward perturbations) were randomly interspersed to reduce anticipatory motor adaptations (ratio 1 to 4).

Once the step threshold was identified, participants completed 40 ramp-and-hold support surface perturbations set at 12cm and ~75%, 85%, and 95% of their step threshold in a randomized fashion (Fig 2, Table 1). To mitigate adaptation and anticipation, participants experienced 8 cm catch trials (e.g., forward perturbations) randomly interspersed within the perturbation set, the same as those experienced when determining the step threshold. A 5-minute seated rest break followed every 20 perturbations to mitigate fatigue.

Data processing

Limb segment marker data and ground reaction forces from both force plates were used for all estimates of joint kinematics and kinetics. Ground reaction forces were filtered using a fourth-order low-pass filter with a 50 Hz cutoff, while marker data was filtered similarly with a 10 Hz cutoff. Inertial artifacts that arise from translating the platform were removed (37, 38). Torques at the ankle, knee, and hip were estimated using the inverse dynamics toolbox in OpenSim (Gait 2892 model) (39). We calculated horizontal CoM acceleration as the ground reaction forces divided by the participant's mass minus platform acceleration. CoM displacement and velocity were calculated as the weighted sum of all segmental masses from the kinematic data as previously done (24, 26, 40, 41). CoM displacement and velocity were taken relative to the movement of the platform, similar to CoM acceleration. CoM displacement and velocity were up-sampled using linear interpolation to 1000 Hz for all further analysis.

All EMG data were high-pass filtered using a third-order zero-lag Butterworth filter with a 35 Hz cutoff. They were then demeaned, rectified, and low-pass filtered (40 Hz) (26). EMG signals were then normalized by the peak activity over all analyzed trials, yielding a value between 0 and 100.

Perturbation trials that elicited a stepping response or trials where participants uncrossed their arms were excluded from further analyses. Stepping responses were identified as trials in which the magnitude of ground reaction forces for either leg dropped below 10 N.

Sensorimotor response model (SRM)

To test our hypothesis that the CoM kinematics modulate the multi-joint reactive torque response to postural perturbations, we modified the previously developed EMG-SRM to reconstruct ankle, knee, and hip torque (2, 24, 26, 31, 40). The previously developed EMG-SRM reconstructs reactive muscle activations as a linear combination of CoM kinematics at a common delay (Eq 1).

$$EMG_i = k_d\boldsymbol{d}(t-\lambda) + k_v\boldsymbol{v}(t-\lambda) + k_a\boldsymbol{a}(t-\lambda) \quad (1)$$

where k_d, k_v, and k_a are the feedback gains on CoM displacement (d), velocity (v), and acceleration (a), and λ is the time delay. We note that CoM kinematics represent the deviation of the CoM from a steady-state trajectory relative to the base of support (e.g., the feet), where during standing balance, any change of the CoM resulting from the perturbation is the CoM deviation.

We made two main modifications to this model so it could reconstruct joint torques (Fig 3). The EMG-SRM was developed to examine muscle-level responses, which only contribute to one direction, as muscles can only pull. In contrast, joint torques represent the net effect of the activation of all the muscles that span that joint. This has two implications. First, the torque response (the output) has positive and negative components corresponding to the agonist and antagonist muscle activity. Second, the agonist and antagonist muscle activity is activated differently by the acceleration and braking of the CoM (the input) responses (e.g., agonist muscles are activated in response to CoM acceleration while antagonist muscles respond to CoM braking) (41). Thus, to capture these aspects of the response, parallel loops were added to capture the positive and negative torque response and to predict the torque response to both CoM acceleration and braking (e.g., the positive and negative components of the input; Fig 3). Ultimately, for all joints, the torque-SRM had a maximum of four loops, each with independent gains and delays (Fig 3), resulting in the following general equation:

$$Trq_i = (k_{d1}\boldsymbol{d}(t-\lambda_1) + k_{v1}\boldsymbol{v}(t-\lambda_1) + k_{a1}\boldsymbol{a}(t-\lambda_1)) + (k_{d2}\boldsymbol{d}(t-\lambda_2) + k_{v2}\boldsymbol{v}(t-\lambda_2) + k_{a2}\boldsymbol{a}(t-\lambda_2)) + (k_{d3}\boldsymbol{d}(t-\lambda_3) + k_{v3}\boldsymbol{v}(t-\lambda_3) + k_{a3}\boldsymbol{a}(t-\lambda_3)) + (k_{d4}\boldsymbol{d}'(t-\lambda_4) + k_{v4}\boldsymbol{v}'(t-\lambda_4) + k_{a4}\boldsymbol{a}'(t-\lambda_4)) \quad (2)$$

where k_d, k_v, and k_a are the feedback gains on CoM displacement (d), velocity (v), and acceleration (a), and λ is the time delay, and a', v', and d' represents the braking of the CoM. Note that EMG data is not used in the Torque-SRM model.

We tuned the gains and delays within each loop to optimize the fit for each participant and perturbation magnitude. All optimizations were performed in Matlab R2022a (Mathworks, Natick, MA) and used the interior point algorithm implemented in *fmincon.m*. First, the trials at the same perturbation magnitude were averaged for use in all further analyses. Next, the background torque was identified as the mean torque one-second proceeding the onset of the perturbation, and this was removed from the overall torque response prior to SRM fitting as we are interested in evaluating the torque arising from agonist and antagonist muscles in response to the perturbation. For the two SRM loops reconstructing either the positive or negative torque responses, a single, optimization was performed to identify k_{di}, k_{vi}, $k_{ai,}$ and λ_i (where i indicates the ith SRM loop). Bounds were placed on each loop to prevent the algorithm from searching outside a physiologically relevant space, and to prevent the loops from reconstructing the same features within the response (Supplemental Table 1). These bounds were determined heuristically and were the same for all subjects. During the fitting process, the fit of each loop was evaluated. If the loop poorly fit the data, hand-tuning optimization was used to adjust the bounds to achieve the best model fit (e.g., the highest R^2 and variance accounted for (VAF)). After the two separate optimizations identified the best values of the parameter sets, the gains and delays were concatenated into an initial guess for a final optimization. The final optimization concurrently optimized the gains for both loops with the lower and upper bounds for the gain parameters set at ± 10% of the initial optimization, and the bounds for the delay parameters set at ± 10ms of the initial optimization. During the fitting, we found four loops were required to reconstruct the reactive hip torque, and three loops were required at the knee and ankle, where loops were removed post-hoc if the gains for the entire loop were zero (Fig 5, 7 & 9). For brevity, the data presented are only for the left leg, and the results were similar when examining the torque and subsequent SRM fits in the right leg.

Statistical analysis

We quantified how well the torque-SRM could reconstruct the reactive joint torques. We quantified the similarity between the inverse dynamics (ID)-derived joint torques and the SRM reconstructed joint torques using R^2 (squared center Pearson's correlation coefficient) and VAF. VAF was defined as the square of Pearson's uncentered correlation coefficient (42), as has been done in previous studies (26, 40, 41). Both R^2 and VAF are necessary to evaluate the goodness of fit between the inverse dynamics (ID)-derived joint torques and the SRM reconstructed joint torques (25). The R^2 is high when the torque-SRM captures temporal changes in joint torque response, but less sensitive to errors in the magnitude. In contrast, the VAF is high when the torque-SRM captures the magnitude of the torque response, but is less sensitive to errors in the contour. We also estimated the root mean square error (RMSE) between the ID torque and the SRM reconstructed torque. The RMSE was normalized by the range of the ID torque.

We evaluated how the feedback gains changed as a function of perturbation magnitude. We compared the magnitude of the feedback gains and delays using a linear mixed effects model for each joint and each gain or delay. Perturbation magnitude was treated as a fixed factor, while subject was treated as a random factor. For all models, we used a restricted maximum likelihood method to approximate the likelihood of the model and Satterthwaite corrections for degrees of freedom (43). These adjustments reduce Type 1 errors, even for small sample sizes (43). We performed all statistical analyses in MATLAB R2022a. Significance was set *a priori* at $\alpha = 0.05$. We used Bonferroni post hoc corrections for multiple comparisons. All metrics are reported as the mean ± standard deviation unless otherwise noted.

RESULTS

A center of mass-driven sensorimotor response model accurately predicts the reactive multi-joint torque response to perturbations

The SRM qualitatively reconstructed the time history of the torque response at the hip, knee, and ankle at all perturbation magnitudes, capturing the salient features of the response (Fig 4 A, B & C). For example, in the reactive torque response at the hip, we were able to capture both flexion peaks immediately after perturbation onset, as well as the later extension peak (Fig. 4A). The torque-SRM captured peaks in knee and ankle torques as well (Fig 4 B & C). Notably, for

all joints, the SRM also captured the torque response after the ramp perturbation ended (>~0.5 seconds), and could capture all salient features up to 2.5 seconds after the perturbation (the longest time after the perturbation we could evaluate).

Quantitatively, the SRM accurately predicted the entire time course of the reactive torque response at all perturbation magnitudes at the hip, knee, and ankle (Fig 4 D, E & F). Across all perturbation magnitudes and joints, the SRM was able to accurately reconstruct the ID-derived reactive joint torques, with high R^2 (*Ankle:* mean: 0.95 ± 0.03, min: 0.88; *Knee:* mean: 0.94 ± 0.04, min: 0.83; *Hip:* mean: 0.94 ± 0.04, min: 0.79) and VAF (*Ankle:* mean: 0.99 ± 0.01, min: 0.96; *Knee:* mean: 0.97 ± 0.04, min: 0.85; *Hip:* mean: 0.95 ± 0.04, min: 0.82). Moreover, the root mean squared error (RMSE) was low at all joints and magnitudes (*Ankle:* mean: 7 ± 2%, max: 11%; *Knee:* mean: 5 ± 2%, max: 9%; *Hip:* mean: 4 ± 2%, max: 9%).

A center of mass-driven sensorimotor response model dissociates the feedforward and feedback contributions to the multi-joint reactive torque response

Based on the delays associated with each loop within the SRM, we dissociated feedforward and feedback torque responses, as well as different feedback response pathways at each joint. In this section we discuss differences in the feedforward and feedback contributions at each joint, all driven by task-level feedback of CoM deviations.

Hip Response: Four loops were required at the hip to fit the reactive torque response, with a feedforward loop corresponding to either the acceleration and braking of the CoM, and two feedback loops (Fig 5). The first SRM loop was driven by the acceleration of the CoM at the onset of the ramp perturbation and captured the initial flexion torque at the onset of the perturbation and occurred at nearly a "zero-delay" (average λ_1 = 1 ± 1 ms across all perturbation magnitudes) prior to neurally-mediated reactive muscle activation (Fig 2). This initial torque response from the hip flexors is counter to the required balance-correcting response to a backward support surface perturbation. Because the CoM is pushed forward, a reactive torque response from the posterior chain muscles is required to maintain balance (44). The second hip flexion peak was driven by the acceleration of the CoM at the onset of the ramp perturbation and captured by a second feedback loop with a "late delay" (average λ_2 = 160 ± 84 ms across all perturbation magnitudes; Fig 5). The third SRM loop captures the majority of the hip extension

torque response. It was driven by CoM displacement and velocity and had a "late delay" (average λ_3 = 329 ± 74 ms across all perturbation magnitudes; Fig 5). A hip extension torque is the expected torque response from posterior chain muscles that will stabilize the body (44). The final loop captured the peak in hip extension that was driven by the braking of CoM at the end of the ramp perturbation and occurred at a "zero-delay" loop (average λ_4 = 6 ± 9 ms across all perturbation magnitudes; Fig 5).

Across all loops, the delays (λ) did not significantly vary across perturbation magnitudes; however, gains within the first loop did vary (Fig 6). There was a modest, but significant, difference in K_{A1} during the smallest perturbation (e.g., 12cm) compared to all other perturbations. K_{A1} was 7% ($p=0.004$), 8% ($p<0.001$), and 9% ($p<0.001$) lower during the 12cm perturbation compared with the perturbation at 75, 85, and 95% of the step threshold, respectively. The difference in the K_{A1} gain likely indicates a scaling of the feedforward short-range stiffness response with perturbation magnitude. No other gains varied significantly with perturbation magnitude.

Knee Response: The torque response at the knee was captured by three loops, two feedforward loops driven by the acceleration and braking of the CoM, and one feedback loop (Fig 7). The first SRM loop was driven by the acceleration of the CoM at the onset of the ramp perturbation and captured the initial extension torque that occurred at nearly a "zero-delay" (average λ_1 = 1 ± 2 ms across all perturbation magnitudes). The second loop captured a majority of the knee flexion torque response. It was driven by CoM displacement and velocity and had a "late delay" (average λ_2 = 213 ± 93 ms across all perturbation magnitudes; Fig 7). The third loop captured the peak in the knee flexion torque that was driven by the braking of CoM at the end of the ramp perturbation, and occurred at a "zero-delay" loop (average λ_3 = 4 ± 9 ms across all perturbation magnitudes; Fig 7).

Across all knee torque loops, the delays (λ) did not significantly vary across perturbation magnitudes; however, the gains did vary within the first loop (Fig 8). There was a modest, but significant decrease in K_{A1} during the 12cm perturbation compared with the perturbation at 85 and 95% of the step threshold (*12cm vs. 85%*: difference = 10%, p = 0.008; *12cm vs. 95%*: difference = 12%, p = 0.004). It was also significantly lower during the 75% perturbation compared to the perturbation at 95% of step threshold (difference = 4%, p = 0.003). K_{V1} was

significantly higher during the 75% perturbation compared to the perturbation at 95% of step threshold (difference = 41%, p = 0.003). Lastly, K_{D1} was significantly higher during the 12cm perturbation compared with the perturbation at 75, 85, and 95% of the step threshold (*12cm vs. 75%*: difference = 200%, p < 0.001, *12cm vs. 85%*: difference = 200%, p < 0.001, *12cm vs. 95%*: difference = 200%, p < 0.001). These differences may reflect a scaling of the feedforward short-range stiffness response with perturbation magnitude. No other gains varied significantly with perturbation magnitude.

Ankle Response: In contrast to the hip and knee, the response at the ankle only required feedback contributions, with one "early" feedback loop and two "late" feedback loops (Fig 9). Most notably, there was no "zero-delay" feedforward component in the ankle torque response. The first loop captured a majority of the plantarflexion response. It was driven by CoM displacement and velocity and had an "early delay" (average λ_1 = 85 ± 23 ms across all perturbation magnitudes; Fig 9). A plantarflexion torque is the expected torque response from posterior chain muscles that will stabilize the body (44). The second loop captured the first peak in ankle plantarflexion. Interestingly, it was driven by CoM acceleration, but was a "late delay" loop (average λ_2 = 190 ± 44 ms across all perturbation magnitudes).

The velocity gain in the first loop (K_{V1}), as well as the delay of the second loop (λ_2), significantly varied across perturbation magnitudes (Fig 10). K_{V1} was significantly higher during the 12cm perturbation compared with the perturbation at 95% of the step threshold (difference = 73%; p = 0.005). It was also higher during 75% compared with 95% of the step threshold (difference = 51%; p = 0.004). As gains do not typically decrease as perturbation magnitude increases, this may represent a saturation of CoM velocity in the ankle response. There was a modest, but significant difference in λ_2 during the 75% compared with 95% of the step threshold perturbations (difference = 4%, p = 0.008).

DISCUSSION

Our work provides novel insight into how neurally-mediated feedforward and feedback pathways contribute to the overall multi-joint torque response, supporting our secondary hypothesis that a torque-SRM could differentiate feedforward (the instantaneous “mechanical feedback” muscle short-range stiffness) torque from the feedback torque that is generated

through sensorimotor transformations at each joint. Our results also indicate that the reactive torque response at the hip, knee, and ankle can be robustly described by sensorimotor feedback of center of mass kinematics, supporting the established hypothesis that the nervous system uses task-level variables to drive the coordinated multi-joint response (2, 22, 28, 31). Interestingly, the pathways contributing to the overall response varied at each joint, indicating that while a task-level variable, CoM kinematics, drives the torque response, the response is joint-specific. Variation between joints may be attributed to differences in musculotendon mechanical properties between proximal and distal joints, as well as differences in the elicited sensory feedback pathways. For example, at the hip and knee, we found a feedforward torque response to the acceleration and braking of the CoM, as well as "late" feedback responses. In contrast, at the ankle, we only observed feedback contributions, with one being an "early" response and the others being "late" feedback responses. The lack of a feedforward contribution at the ankle may be driven by the compliance of the Achilles tendon, which attenuates the intrinsic mechanical response from muscle short-range stiffness. Differentiating the feedforward and feedback contributions at each joint can aid in our understanding of how each joint contributes to the balance-correcting response and how the response can be modulated. It can also aid in identifying disrupted pathways that result in impaired balance in older adults or those with neuromuscular injuries or diseases. Lastly, the ability to mimic the physiological balance-correcting torque response may aid in developing legged robots and wearable robotic devices that can withstand and help the user withstand postural perturbations, respectively.

Feedforward contributions to the reactive torque differ across joints

The "zero-delay" feedforward torque presumably arises from the intrinsic mechanical properties of the musculoskeletal system, namely muscle short-range stiffness. The initial torque response at the hip and knee occurs prior to muscle activation (Fig 2) and, thus, cannot be driven by neurally mediated feedback pathways. Furthermore, the muscle short-range stiffness response is an instantaneous response to an imposed stretch, and within each joint, we see a small deflection of joint angle ~1 deg within the first 50ms that could cause the muscle-tendon unit to stretch (Fig 2). We thus attribute the initial “zero-delay” hip torque response (Fig 5: Loop #1) to the intrinsic properties of hip flexor muscles, due to the initial extension of the hip, and the initial zero-delay knee torque response (Fig 7: Loop #1) to the intrinsic properties of knee extensor

muscles, due to the initial flexion of the knee. Clearly identifying the mechanism underlying the second feedforward loop at the hip and knee at the deceleration of the ramp and hold perturbation (Loops #4 and #3, respectively), is more difficult because of the ongoing feedback muscle activity in response to the initial acceleration of the perturbation. However, we still attribute this response to muscle short-range stiffness because 1) there is no clear burst in muscle activation from hip extensors or knee flexors (e.g., biceps femoris) that could drive this response (Fig 2), and 2) the characteristics of this loop are the same as Loop #1 (e.g., primarily driven by CoM acceleration, the latencies are similar, and the sign of the torque response maps to the sign of CoM acceleration in the same manner). Lastly, it is worth highlighting that the same muscles may elicit feedforward torque responses at the hip and knee because biarticular muscles that flex the hip also extend the knee (e.g., acceleration – rectus femoris) and the biarticular muscles that extend the hip also flex the knee (braking – biceps femoris), thus providing a short-range stiffness response at both joints with similar delays.

While global changes in CoM kinematics drive the feedback neural responses, as has been shown previously (26, 45-47), it is highly probable that CoM kinematics do not directly drive the feedforward muscle short-range stiffness response; rather, it is driven by a local stretch of the muscle. Muscle short-range stiffness is elicited by a stretch within the muscle (e.g., a local signal) (12), and there is no transformation from sensory input to a torque output like the feedback response and the physiological principle underlying the torque-SRM. One of the biggest limitations when exploring if global versus local signals drive the feedforward muscle short-range stiffness response is the lack of a sensitive measure of the initial length change in muscle or the initial angular acceleration at the joints. However, due to inter-joint coupling and induced accelerations, when a balance perturbation is applied, the induced angular acceleration propagates through all the joints and to the CoM simultaneously (48). Thus, while, CoM acceleration may not be the physiological driver of the muscle short-range stiffness response, it can be used as a proxy measure of joint angular accelerations (e.g., angular acceleration or the initial stretch with the muscles is correlated with CoM acceleration).

Distal tendons that are more compliant may attenuate the muscle short-range stiffness response, leading to the lack of feedforward response at the ankle. At the hip and knee, we observed "zero-delay" feedforward loops, while a "zero-delay" loop was not present at the ankle (Fig 5, 7, & 9). The magnitude of the short-range stiffness response is sensitive to the amplitude

of the stretch within the muscle (12). Due to the serial connection between muscle and tendon, the stretch that occurs within each muscle during the imposed perturbations will be dependent upon the compliance of the tendon to which it is attached, with more stretch occurring within the tendon when it is more compliant than the muscle. Our results suggest that, at the ankle during postural conditions, since the tendon is less stiff than the muscle at nearly all levels of muscle activation (49-51), a majority of the perturbation-related stretch occurs within the tendon, attenuating the short-range stiffness response within the muscle, resulting in no "zero-delay" feedforward component at the ankle. In contrast, at the hip and knee, which are thought to have stiffer tendons (52), most of the imposed stretch occurs within the muscle, resulting in the "zero-delay" feedforward torque. This result is supported by prior musculoskeletal modeling work that found that including muscle short-range stiffness within the model resulted in hip and knee torques being generated prior to muscle activation but not ankle torques (29). We note the small rise in ankle torque at the time of the perturbation that is unaccounted for in our current model. However, even if we implemented a "zero-delay" loop, it was unable to capture this response. This could be due to non-linear musculotendon mechanics that our linear model was unable to capture.

Differences in tendon stiffness between the proximal and distal joint may also impact the efficacy of using feedforward control, and the lack of a "zero-delay" feedforward torque response at the ankle has important implications for balance control. Feedforward modulation of muscle activity or co-contraction is thought to increase muscle stiffness, thereby increasing the resultant feedforward torque, which can improve postural stability by providing greater instantaneous resistance to unexpected perturbations (7, 8). However, our results suggest that feedforward modulation at the ankle may be an ineffective way to improve postural stability. Due to the compliance of the Achilles tendon relative to that of the triceps surae (49-51), feedforward increases in muscle activation would result in a minimal increase in the resultant ankle torque that arises from muscle short-range stiffness. This is in agreement with previous findings that ankle stiffness is insufficient to maintain postural stability (19, 21). In contrast, since the tendons at the hip and knee are likely less compliant than the Achilles tendon (52), increasing muscle activation or co-contraction at the hip or knee may be an effective way to increase the feedforward torque response.

Feedback contributions to the reactive torque differ across joints

While a global change in CoM drives the feedback response at each joint, our results suggest that different neural mechanisms may modulate the feedback responses across the hip, knee, and ankle. Through the use of the torque-SRM, we separated the feedback pathways into "early" and "late" components based on the time delays of each loop (Fig 5, 7 & 9). These results vary from previous findings where the same CoM kinematics transformation, with a single delay, could predict the coordinated muscle activity across different joints (53). However, this model only had a single delay consistent with the sub-cortical response. It was recently observed that implementing a parallel loop EMG-SRM to fit medial gastrocnemius activation could capture both cortical and sub-cortical contributions, significantly improving the overall fit (27). If reactive EMG signals at the ankle arise from both cortical and sub-cortical pathways, so would the resultant ankle torque, as we found in our study. Interestingly, the same cortical and sub-cortical pathways do not appear to be modulating the resultant torques across joints. For example, at the hip, one feedback pathway is likely transcortical (average delay of 160 ± 84 ms) while the other may be a voluntary response (average delay of 329 ± 74 ms; Fig 6) (27, 54). In contrast, at the ankle, there was an "early" loop (λ_1 = 85 ± 23 ms) that was likely a spinal or brainstem mediated pathway, while the "late" loop is likely a transcortical pathway (λ_2 = 190 ± 44 ms) (1, 27, 54). While we can speculate on the neural origin of each feedback pathway, definitively identifying the sensory feedback pathway for each loop was outside the scope of this study and requires future investigation.

Limitations

One limitation of the current study is that only a single perturbation direction (backward support surface translations) was tested. Due to differences in musculotendon architecture, the feedforward contribution may vary with perturbation direction. The torque-SRM's ability to predict joint torque has only ever been evaluated in the sagittal plane (28). Thus, it is unclear if the torque-SRM can predict frontal plane joint torques. While the EMG-SRM has accurately predicted reactive muscle activations during frontal plane perturbations (23), future work should include testing the efficacy of the torque-SRM at capturing frontal plane torques.

The perturbations tested were also large (at 95% of the step threshold). The response to these perturbations required both a hip and ankle strategy, even during the smallest applied

perturbation (12cm). It remains to be seen if the torque-SRM introduced in this study is robust during smaller perturbations that mainly require an ankle strategy. Additionally, the participants were instructed to maintain a foot-in-place balance response, even to the largest applied perturbations. Since the perturbations were close to the participant's step threshold, it is possible that the natural response would have been to take a step. Additional testing is required to determine if the torque-SRM can accurately predict the reactive joint torques when a step is taken.

Future implications and conclusions

The ability to differentiate the feedforward and feedback contributions, as well as the different feedback pathways that are contributing to the overall multi-joint torque response, may provide a framework for determining mechanisms underlying the impaired control of balance in aging, injury, or neuromuscular pathology. For example, older adults have decreased Achilles tendon stiffness (55-57), and an increase in the delay of the feedback pathways (58-60). This methodology could differentiate the impact of these changes on the overall balance-correcting response. Once the deficit is identified, targeted training at the source of the impairment can be developed. This is critical since training or treatment targeted at neural deficits (e.g., sensory feedback delays) will vary from training targeted at biomechanical deficits (e.g., tendon stiffness). This same framework could be used to identify specific deficits in individuals with Parkinson's disease, older adults with mild cognitive impairment, stroke survivors, or other neuromuscular injuries and diseases. To implement this method in other populations, measures of CoM kinematics (input into the torque-SRM), and joint torque (output of the torque-SRM) are required. It is also worth noting that the number of trials collected within this study is similar, if not lower, than the number of trials we have previously collected within clinical populations (41, 61), supporting the feasibility of this approach.

Moreover, our method may provide a means to differentiate feedforward from feedback adaptation. Based on our experimental design with catch trials, we did not anticipate feedforward adaptations, including changes in pre-perturbation muscle activation or postural changes. However, in prior work, sensorimotor adaptation (e.g., a change in the feedback gains) was observed when the same perturbation was repeatedly applied. It is worth highlighting that within this prior study, there were either no or modest changes in feedforward components, including

548 background muscle activation and posture (24). However, it is difficult to quantify feedforward
549 changes in muscle activation from experimental data, and muscle intrinsic torque responses
550 arising from neurally mediated feedforward activation of muscles are not accounted for in the
551 EMG response to a perturbation. Our method, which can distinguish the feedforward from the
552 feedback contributions, may be able to assess anticipatory feedforward adaptation from
553 sensorimotor feedback adaptation quantitatively.

554 Our framework may also simplify the control of legged bi-pedal robots, and lower-limb
555 prostheses and exoskeletons. Our framework uses CoM kinematics, a single control signal, to
556 predict the entire time course of the torque response at the ankle, knee, and hip. This one-to-
557 many mapping, rather than the one-to-one mapping currently employed, could simplify the
558 control of these devices. Moreover, using a physiologically-inspired control scheme, where the
559 controller mimics the biological feedforward and feedback responses to postural perturbations,
560 may also improve the embodiment of devices. The principles of embodiment suggest that robotic
561 devices should coordinate with the human's natural response, such that the nervous system can
562 model the controller of the robotic device (62). Since a torque-SRM control scheme would be
563 based on the nervous system's response, very little learning might be required for the human to
564 model the controller. This could ultimately improve device acceptance and usage in the real
565 world.

566

567 **SUPPLEMENTAL MATERIAL**

568 Supplemental material is available at:

569 https://osf.io/gk2ns/?view_only=cee1a8853b2e46c7a78d7afdb42c9748

570

571 **DATA AVAILABILITY**

572 The data from the current study are available from the corresponding author upon reasonable
573 request.

574

575 **GRANTS**

576 This publication was supported by grant number 2127509 from the NSF and American
577 Society for Engineering Education, National Institutes of Health grants F32 AG063460, R01
578 HD046922, R01 HD090642, and McCamish Parkinson's Disease Innovation Program. Its
579 contents are solely the responsibility of the authors and do not necessarily represent the official

views of the National Science Foundation, American Society for Engineering Education, National Institutes of Health, or McCamish Foundation.

DISCLOSURES

The authors declare no conflicts of interest, financial or otherwise.

AUTHOR CONTRIBUTIONS

G.M., O.N.B., K.L.J., and L.H.T. conceived and designed research; G.M. and O.N.B. performed experiments; K.L.J analyzed data, K.L.J., G.S.S., and L.H.T interpreted results of experiments, K.L.J prepared figures and drafted manuscript, K.L.J., G.M., O.N.B., G.S.S., and L.H.T. approved final version of manuscript

FIGURES

Figure 1. Schematic of the balance correcting response. The torque response to postural perturbations at each joint is mediated by the neurally-mediated feedforward pathways, where the torque produced at the time of the perturbation ($\lambda \sim 0$ ms), as well as neurally-mediated sub-cortical ($50 < \lambda < 150$ ms) and cortical ($\lambda > 150$ ms) pathways.

Figure 2. Experimental protocol from a representative participant. Participants were instructed to maintain a foot-in-place balance response to perturbations at 4 magnitudes: 12cm, and 75%, 85%, and 95% of their step threshold. Joint kinematics and kinetics were estimated using the OpenSim Gait 2892 model (39). All torques and angles represent the change in torque from the baseline, pre-perturbation value. The dashed line indicates the start of the perturbation. CoM = center of mass, DF = dorsiflexion, PF = plantarflexion, Ext = extension, Flex = flexion, Sol = soleus, TA = tibialis anterior, BF = biceps femoris, RF = rectus femoris, GM = gluteus medius.

Figure 3. Torque sensorimotor response model (SRM). The SRM predicted joint torque as the quasi-linear sum of CoM deviation (acceleration, a; velocity, v; and displacement, d). We added parallel SRMs, each with independent gains and delays, to predict the torque response. The parallel loops enabled us to predict the positive and negative components of the torque response as well as the torque response to CoM acceleration and braking. Note that this is the model for the hip flexion torque response.

Figure 4. Across all joints, the SRM could accurately reconstruct the torque response at the hip, knee, and ankle. (A - C) Representative fits for the CoM-driven torque-SRM for all perturbation magnitudes (12cm, and 75%, 85%, and 95% of step threshold). The dashed line indicates the start of the perturbation; the SRM fit is in purple, with the ID-derived torque in black. PF = plantarflexion, Flex = flexion, Ext = extension. (D - F) The SRM reconstructed the ID-derived torques well at all joints across all perturbation magnitudes. Moreover, there was a low root mean squared error (RMSE) at all joints at all perturbation magnitudes (e.g., <~10%) between the SRM reconstructed and ID torques. The purple dots represent the group means and standard deviation, while the gray dots and lines represent each participant.

Figure 5. Multi-loop SRM at the hip for a perturbation at 95% of step threshold from a representative participant. At the hip, the balance-correcting torque response is mediated by two feedforward components (red), corresponding to the acceleration and braking of the center of mass, and by two "late" feedback components (blue) with delays longer than 150 ms. The SRM included two loops for any positive change in torque from the baseline and two loops for any negative change in torque from the baseline. The loops are summed, resulting in the overall torque response (purple).

Figure 6. Sensorimotor response model (SRM) gains at the hip for each perturbation magnitude. Each loop was separated into feedforward contribution (red), early feedback contribution (green), or late feedback contribution (blue) based on its delay (λ). K_{Di}, K_{Vi}, and K_{Ai} are the designated SRM gains for CoM displacement, velocity, and

acceleration, respectively, while λ_i designates the time delay, *i* represents the *i*th loop. The dots represent the group means and standard deviation, while the gray dots and lines are each participant. The black line and asterisks indicate a significant difference in the SRM gains or time delays across perturbation magnitudes ($p < 0.05/6$ using Bonferroni corrections for multiple comparisons).

Figure 7. Multi-loop SRM at the knee for a perturbation at 95% of step threshold from a representative participant. At the knee, the balance-correcting torque response is mediated by two feedforward components (red), corresponding to the acceleration and braking of the center of mass, and by one "late" feedback component (blue) with a delay longer than 150 ms. The SRM included one loop for any positive change in torque from the baseline and two loops for any negative change in torque from the baseline. The loops are summed, resulting in the overall torque response (purple).

Figure 8. Sensorimotor response model (SRM) gains at the knee for each perturbation magnitude. Each loop was separated into feedforward contribution (red), early feedback contribution (green), or late feedback contribution (blue) based on its delay (λ). K_{Di}, K_{Vi}, and K_{Ai} are the designated SRM gains for COM displacement, velocity, and acceleration, respectively, while λ_i designates the time delay, *i* represents the *i*th loop. The dots represent the group means and standard deviation, while the gray dots and lines are each participant. The black line and asterisks indicate a significant difference in the SRM gains or time delays across perturbation magnitudes ($p < 0.05/6$ using Bonferroni corrections for multiple comparisons).

Figure 9. Multi-loop SRM at the ankle for a perturbation at 95% of step threshold from a representative participant. At the ankle, the balance-correcting torque response is mediated by one "early" feedback component that has a delay less than 150 ms and one "late" feedback component with a delay longer than 150 ms. Notably, unlike the hip and knee, there is no feedforward component. The SRM included two loops for any positive change in torque from the baseline and one loop for any negative change in torque from the baseline. The loops are summed, resulting in the overall torque response (purple). Note that in some, but not all participants, a third loop was required to capture the negative change in torque from the baseline values; however, it is not shown here.

Figure 10. Sensorimotor response model (SRM) gains at the ankle for each perturbation magnitude. Each loop was separated into feedforward contribution (red), early feedback contribution (green), or late feedback contribution (blue) based on its delay (λ). K_{Di}, K_{Vi}, and K_{Ai} are the designated SRM gains for COM displacement, velocity, and acceleration, respectively, while λ_i designates the time delay, *i* represents the *i*th loop. The dots represent the group means and standard deviation, while the gray dots and lines are each participant. The black line and asterisks indicate a significant difference in the SRM gains or time delays across perturbation magnitudes ($p < 0.05/6$ using Bonferroni corrections for multiple comparisons).

664 **Table 1: Perturbation magnitudes (cm)**

	Mean (std)	Min	Max
75%	16 (2)	13	18
85%	18 (2)	15	20
95%	21 (2)	17	23

665

REFERENCE:

1. **Horak FB, and Macpherson JM**. Postural orientation and equilibrium. *Handbook of Physiology* 1: 255-292, 1996.
2. **Ting LH, van Antwerp KW, Scrivens JE, McKay JL, Welch TD, Bingham JT, and DeWeerth SP**. Neuromechanical tuning of nonlinear postural control dynamics. *Chaos* 19: 026111, 2009.
3. **Lin S-I, and Woollacott MH**. Postural muscle responses following changing balance threats in young, stable older, and unstable older adults. *Journal of motor behavior* 34: 37-44, 2002.
4. **Allum J, Carpenter M, Honegger F, Adkin A, and Bloem B**. Age-dependent variations in the directional sensitivity of balance corrections and compensatory arm movements in man. *The Journal of physiology* 542: 643-663, 2002.
5. **Cui L, Perreault EJ, Maas H, and Sandercock TG**. Modeling short-range stiffness of feline lower hindlimb muscles. *Journal of Biomechanics* 41: 1945-1952, 2008.
6. **Horslen BC, Milburn GN, Blum KP, Simha SN, Campbell KS, and Ting LH**. History-dependent muscle resistance to stretch remains high after small, posturally relevant pre-movements. *Journal of Experimental Biology* 226: 2023.
7. **Carter RR, Crago PE, and Gorman PH**. Nonlinear stretch reflex interaction during cocontraction. *Journal of neurophysiology* 69: 943-952, 1993.
8. **Kearney RE, and Hunter IW**. System identification of human joint dynamics. *Critical Reviews in Biomedical Engineering* 18: 55-87, 1990.
9. **Lakie M, and Campbell KS**. Muscle thixotropy—where are we now? *Journal of applied physiology* 126: 1790-1799, 2019.
10. **Nguyen KD, Sharma N, and Venkadesan M**. Active viscoelasticity of sarcomeres. *Frontiers in Robotics and AI* 5: 69, 2018.
11. **Finley JM, Dhaher YY, and Perreault EJ**. Contributions of feed-forward and feedback strategies at the human ankle during control of unstable loads. *Experimental Brain Research* 217: 53-66, 2012.
12. **Rack PM, and Westbury DR**. The short range stiffness of active mammalian muscle and its effect on mechanical properties. *Journal of Physiology* 240: 331-350, 1974.
13. **Van Wouwe T, Ting LH, and De Groote F**. An approximate stochastic optimal control framework to simulate nonlinear neuro-musculoskeletal models in the presence of noise. *PLOS Computational Biology* 18: e1009338, 2022.
14. **Carpenter MG, Frank JS, Silcher CP, and Peysar GW**. The influence of postural threat on the control of upright stance. *Experimental brain research* 138: 210-218, 2001.
15. **Pienciak-Siewert A, Horan DP, and Ahmed AA**. Role of muscle coactivation in adaptation of standing posture during arm reaching. *Journal of neurophysiology* 123: 529-547, 2020.
16. **Stamenkovic A, van der Veen SM, and Thomas JS**. Fear priming: a method for examining postural strategies associated with fear of falling. *Frontiers in aging neuroscience* 12: 241, 2020.
17. **Wuehr M, Kugler G, Schniepp R, Eckl M, Pradhan C, Jahn K, Huppert D, and Brandt T**. Balance control and anti-gravity muscle activity during the experience of fear at heights. *Physiological reports* 2: e00232, 2014.
18. **Chvatal SA, and LH. T**. Voluntary and reactive recruitment of locomotor muscle synergies during perturbed walking. *Journal of Neuroscience* 32: 12237-12250, 2012.

19. **Morasso PG, and Sanguineti V**. Ankle muscle stiffness alone cannot stabilize balance during quiet standing. *Journal of neurophysiology* 88: 2157-2162, 2002.
20. **Martino G, Beck ON, and Ting LH**. Voluntary muscle coactivation in quiet standing elicits reciprocal rather than coactive agonist-antagonist control of reactive balance. *Journal of Neurophysiology* 129: 1378-1388, 2023.
21. **Loram ID, and Lakie M**. Direct measurement of human ankle stiffness during quiet standing: the intrinsic mechanical stiffness is insufficient for stability. *The journal of physiology* 545: 1041-1053, 2002.
22. **Lockhart DB, and Ting LH**. Optimal sensorimotor transformations for balance. *Nat Neurosci* 10: 1329-1336, 2007.
23. **Safavynia SA, and Ting LH**. Sensorimotor feedback based on task-relevant error robustly predicts temporal recruitment and multidirectional tuning of muscle synergies. *J Neurophysiol* 109: 31-45, 2013.
24. **Welch TD, and Ting LH**. Mechanisms of motor adaptation in reactive balance control. *PLoS One* 9: e96440, 2014.
25. **Welch TD, and Ting LH**. A feedback model explains the differential scaling of human postural responses to perturbation acceleration and velocity. *Journal of neurophysiology* 101: 3294-3309, 2009.
26. **Safavynia SA, and Ting LH**. Long-latency muscle activity reflects continuous, delayed sensorimotor feedback of task-level and not joint-level error. *Journal of neurophysiology* 110: 1278-1290, 2013.
27. **Boebinger S, Payne A, Martino G, Kerr K, Mirdamadi J, McKay JL, Borich M, and Ting L**. Precise cortical contributions to sensorimotor feedback control during reactive balance. *PLOS Computational Biology* 20: e1011562, 2024.
28. **Afschrift M, De Groote F, and Jonkers I**. Similar sensorimotor transformations control balance during standing and walking. *PLoS computational biology* 17: e1008369, 2021.
29. **De Groote F, Allen JL, and Ting LH**. Contribution of muscle short-range stiffness to initial changes in joint kinetics and kinematics during perturbations to standing balance: A simulation study. *J Biomech* 55: 71-77, 2017.
30. **Bingham JT, Choi JT, and Ting LH**. Stability in a frontal plane model of balance requires coupled changes to postural configuration and neural feedback control. *Journal of neurophysiology* 106: 437-448, 2011.
31. **Welch TD, and Ting LH**. A feedback model reproduces muscle activity during human postural responses to support-surface translations. *Journal of neurophysiology* 99: 1032-1038, 2008.
32. **Tankisi H, Burke D, Cui L, de Carvalho M, Kuwabara S, Nandedkar SD, Rutkove S, Stålberg E, van Putten MJ, and Fuglsang-Frederiksen A**. Standards of instrumentation of EMG. *Clinical Neurophysiology* 131: 243-258, 2020.
33. **Van Wouwe T, Afschrift M, Dalle S, Van Roie E, Koppo K, and De Groote F**. Adaptations in reactive balance strategies in healthy older adults after a 3-week perturbation training program and after a 12-week resistance training program. *Frontiers in Sports and Active Living* 3: 714555, 2021.
34. **Beck ON, Shepherd MK, Rastogi R, Martino G, Sawicki GS, and Ting LT**. Artificially Fast ExoBoots Improve Standing Balance While Reducing Initial Feedback Response. In: *International Society for Posture and Gait Research World Congress*. Montreal, Canada,: 2022.

35. **Palmer JA, Payne AM, Ting LH, and Borich MR**. Cortical engagement metrics during reactive balance are associated with distinct aspects of balance behavior in older adults. *Frontiers in Aging Neuroscience* 13: 684743, 2021.
36. **Prins N, and Kingdom FA**. Applying the model-comparison approach to test specific research hypotheses in psychophysical research using the Palamedes toolbox. *Frontiers in psychology* 9: 1250, 2018.
37. **Preuss R, and Fung J**. A simple method to estimate force plate inertial components in a moving surface. *Journal of biomechanics* 37: 1177-1180, 2004.
38. **Hnat SK, van Basten BJ, and van den Bogert AJ**. Compensation for inertial and gravity effects in a moving force platform. *Journal of biomechanics* 75: 96-101, 2018.
39. **Delp SL, Anderson FC, Arnold AS, Loan P, Habib A, John CT, Guendelman E, and Thelen DG**. OpenSim: open-source software to create and analyze dynamic simulations of movement. *IEEE transactions on biomedical engineering* 54: 1940-1950, 2007.
40. **Welch TDJ, and Ting LH**. A Feedback Model Explains the Differential Scaling of Human Postural Responses to Perturbation Acceleration and Velocity. *J Neurophysiol* 101: 3294-3309, 2009.
41. **McKay JL, Lang KC, Bong SM, Hackney ME, Factor SA, and Ting LH**. Abnormal center of mass feedback responses during balance: A potential biomarker of falls in Parkinson's disease. *Plos one* 16: e0252119, 2021.
42. **Zar J**. Biostatistical analysis.,(4th edn)(Prentice Hall: Upper Saddle River, NJ, USA). 1999.
43. **Luke SG**. Evaluating significance in linear mixed-effects models in R. *Behavior Research Methods* 49: 1494-1502, 2017.
44. **Horak FB, and Nashner LM**. Central programming of postural movements: adaptation to altered support-surface configurations. *Journal of neurophysiology* 55: 1369-1381, 1986.
45. **Nashner L**. Adapting reflexes controlling the human posture. *Experimental brain research* 26: 59-72, 1976.
46. **Carpenter MG, Allum JH, and Honegger F**. Directional sensitivity of stretch reflexes and balance corrections for normal subjects in the roll and pitch planes. *Experimental brain research* 129: 93-113, 1999.
47. **Ting LH, and Macpherson JM**. Ratio of shear to load ground-reaction force may underlie the directional tuning of the automatic postural response to rotation and translation. *Journal of Neurophysiology* 92: 808-823, 2004.
48. **van Antwerp KW, Burkholder TJ, and Ting LH**. Inter-joint coupling effects on muscle contributions to endpoint force and acceleration in a musculoskeletal model of the cat hindlimb. *Journal of biomechanics* 40: 3570-3579, 2007.
49. **Jakubowski KL, Ludvig D, Perreault EJ, and Lee SS**. Non-linear properties of the Achilles tendon determine ankle impedance over a broad range of activations in humans. *Journal of Experimental Biology* jeb. 244863, 2023.
50. **de Zee M, and Voigt M**. Moment dependency of the series elastic stiffness in the human plantar flexors measured in vivo. *Journal of biomechanics* 34: 1399-1406, 2001.
51. **Loram ID, Maganaris CN, and Lakie M**. The passive, human calf muscles in relation to standing: the short range stiffness lies in the contractile component. *The Journal of physiology* 584: 677-692, 2007.

52. **Karamanidis K, and Arampatzis A**. Mechanical and morphological properties of human quadriceps femoris and triceps surae muscle–tendon unit in relation to aging and running. *Journal of biomechanics* 39: 406-417, 2006.
53. **Safavynia SA, and LH T**. Task-level feedback can explain temporal recruitment of spatially fixed muscle synergies throughout postural perturbations. *Journal of neurophysiology* 107: 159-177, 2012.
54. **Jacobs JV, and Horak FB**. Cortical control of postural responses. *Journal of Neural Transmission* 114: 1339-1348, 2007.
55. **Stenroth L, Peltonen J, Cronin N, Sipilä S, and Finni T**. Age-related differences in Achilles tendon properties and triceps surae muscle architecture in vivo. *Journal of Applied Physiology* 113: 1537-1544, 2012.
56. **Mademli L, and Arampatzis A**. Mechanical and morphological properties of the triceps surae muscle–tendon unit in old and young adults and their interaction with a submaximal fatiguing contraction. *Journal of Electromyography and Kinesiology* 18: 89-98, 2008.
57. **Coombes BK, Tucker K, Hug F, and Dick TJ**. Age-related differences in gastrocnemii muscles and Achilles tendon mechanical properties in vivo. *Journal of Biomechanics* 110067, 2020.
58. **Mackey DC, and Robinovitch SN**. Mechanisms underlying age-related differences in ability to recover balance with the ankle strategy. *Gait & Posture* 23: 59-68, 2006.
59. **Sturnieks DL, Menant J, Vanrenterghem J, Delbaere K, Fitzpatrick RC, and Lord SR**. Sensorimotor and neuropsychological correlates of force perturbations that induce stepping in older adults. *Gait & Posture* 36: 356-360, 2012.
60. **Baudry S**. Aging changes the contribution of spinal and corticospinal pathways to control balance. *Exercise and Sport Sciences Reviews* 44: 104-109, 2016.
61. **Payne AM, Palmer JA, McKay JL, and Ting LH**. Lower cognitive set shifting ability is associated with stiffer balance recovery behavior and larger perturbation-evoked cortical responses in older adults. *Frontiers in Aging Neuroscience* 13: 742243, 2021.
62. **Hybart RL, and Ferris DP**. Embodiment for Robotic Lower-Limb Exoskeletons: A Narrative Review. *IEEE Transactions on Neural Systems and Rehabilitation Engineering* 2022.

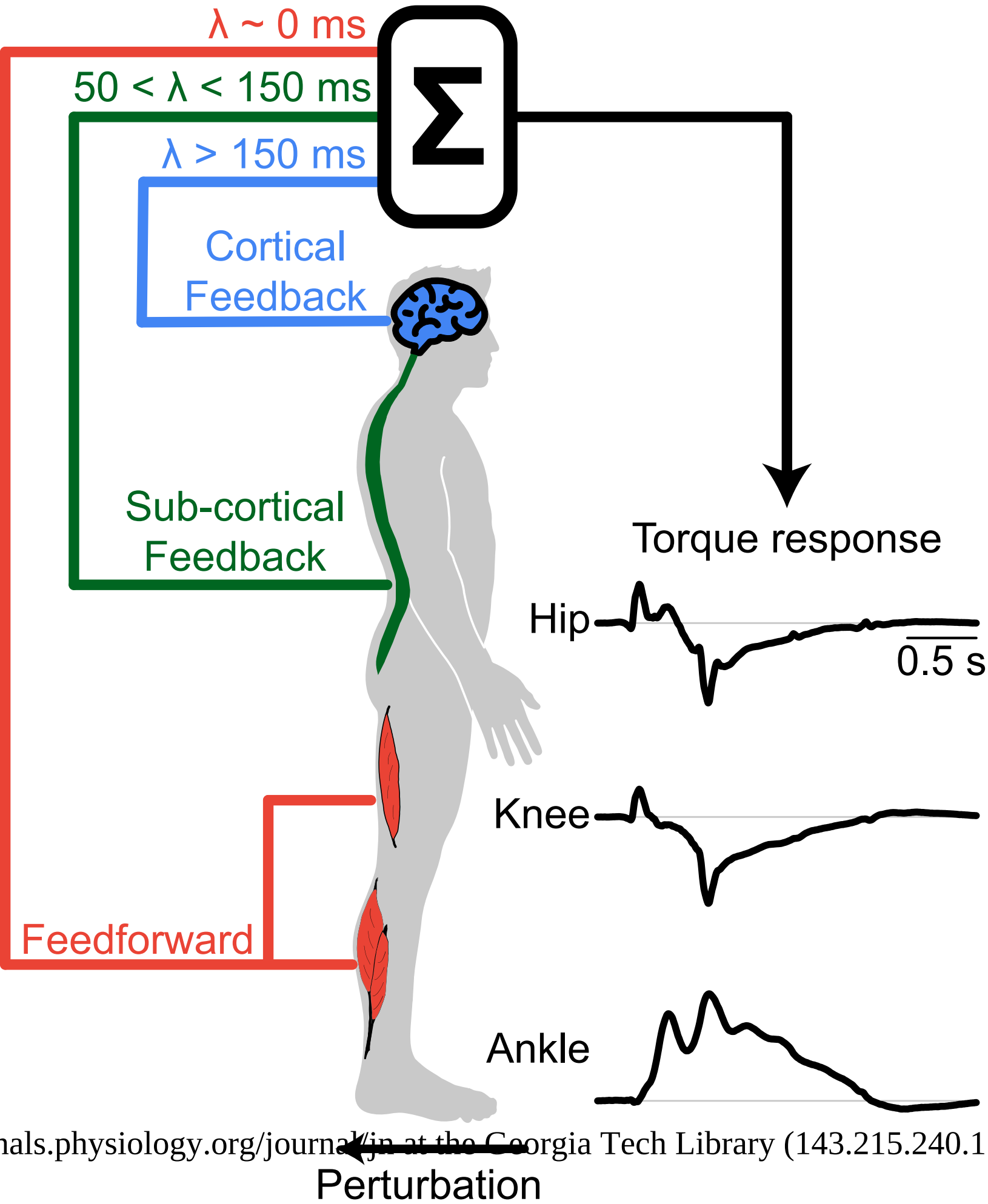

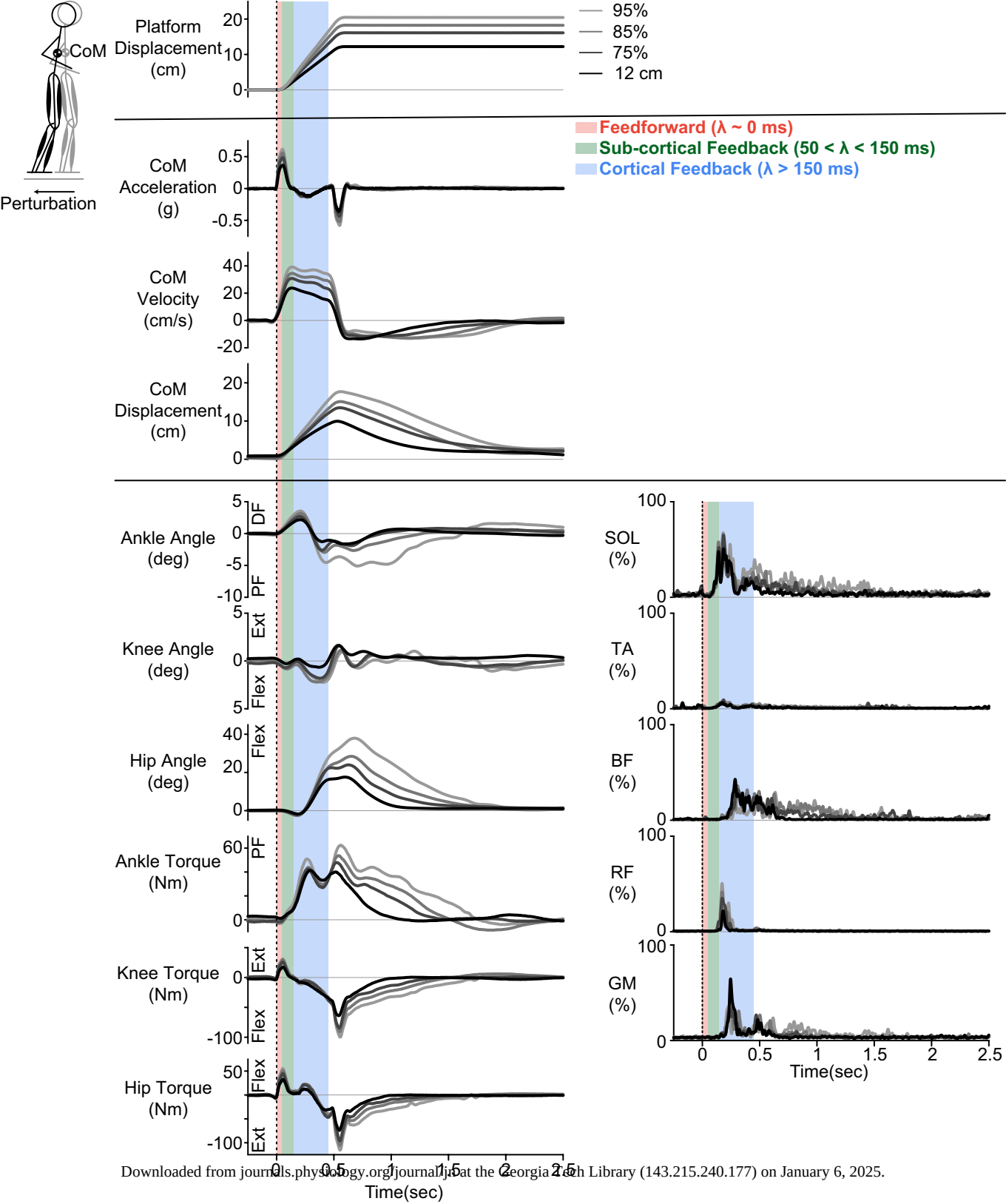

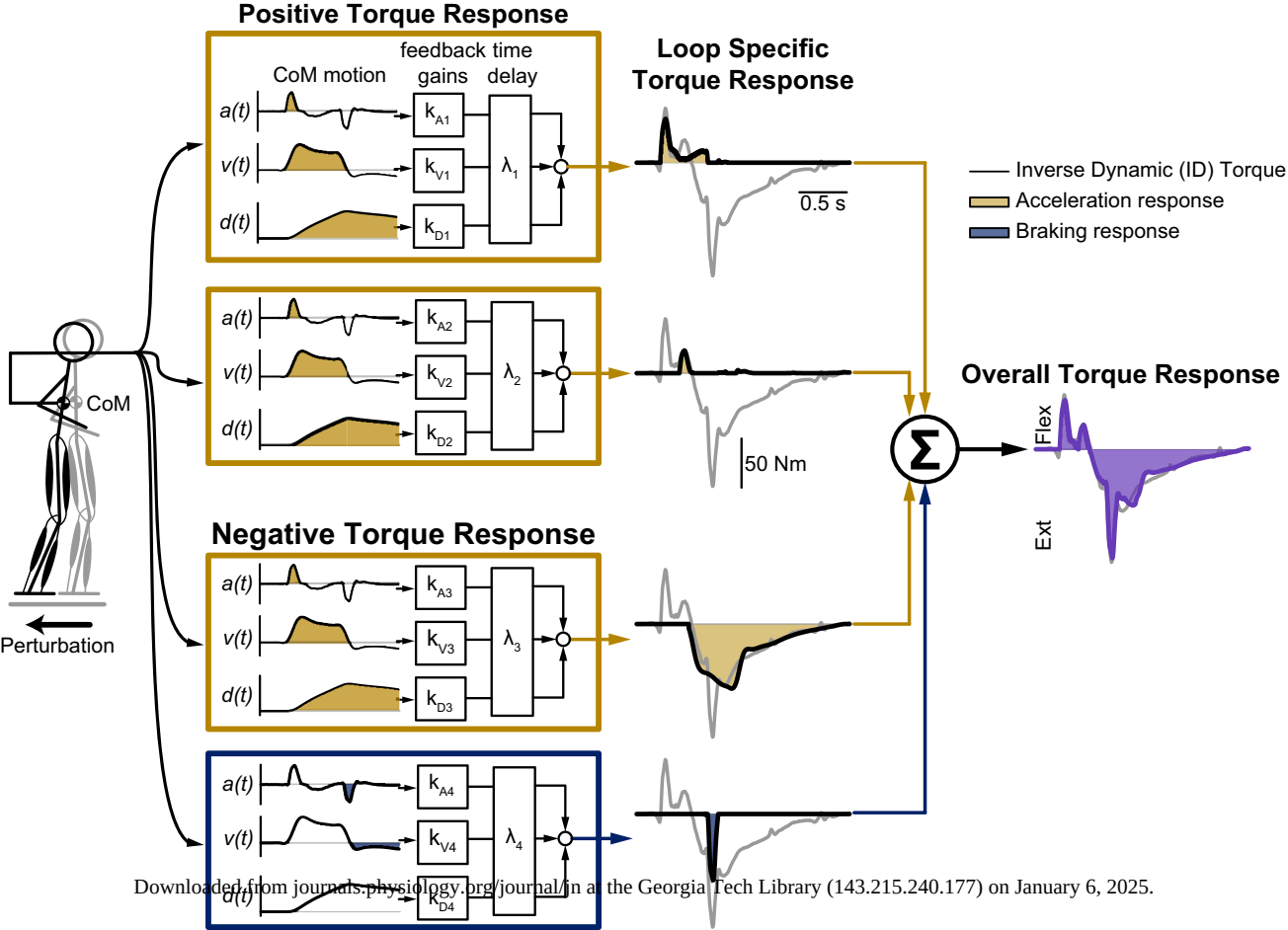

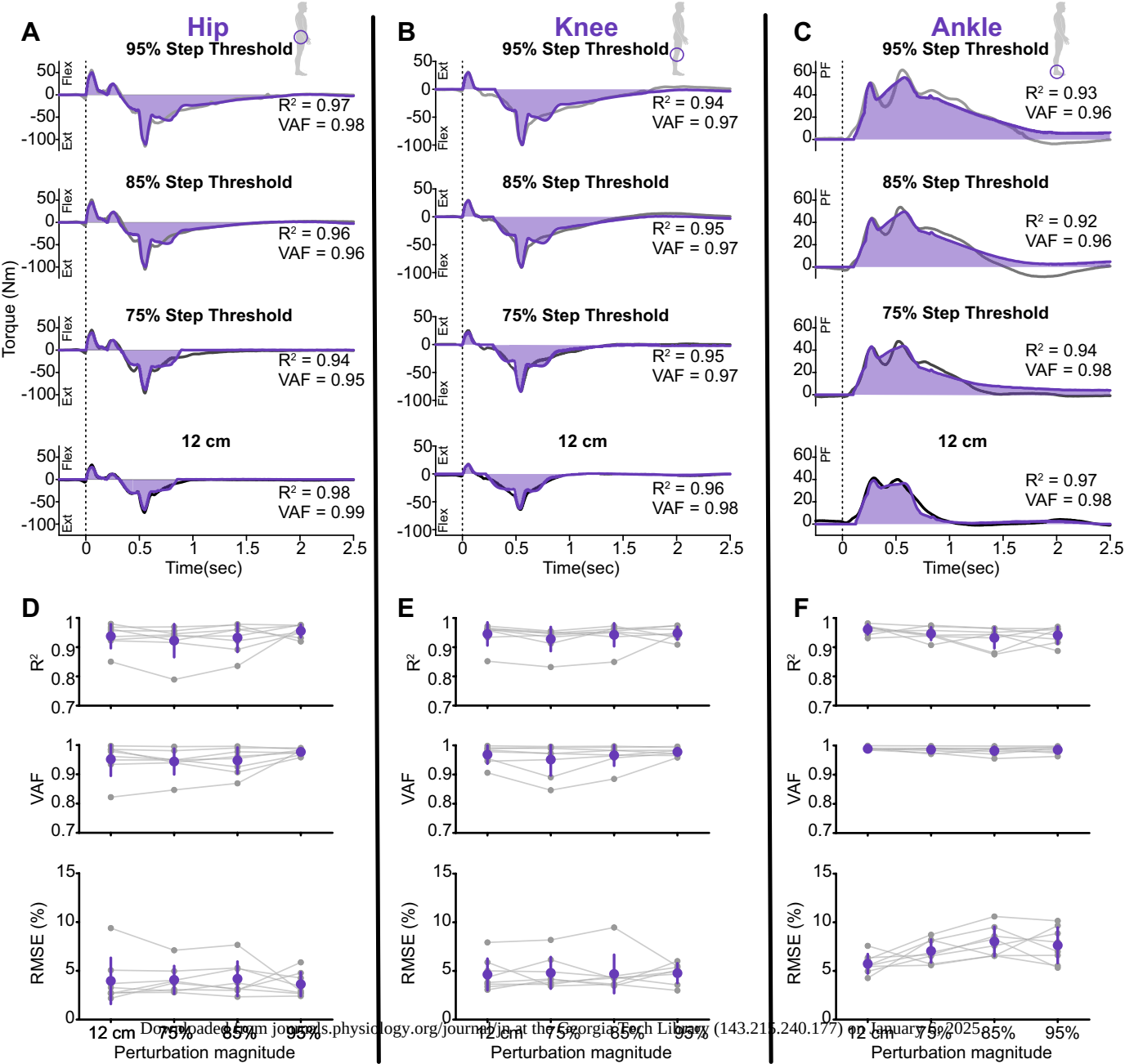

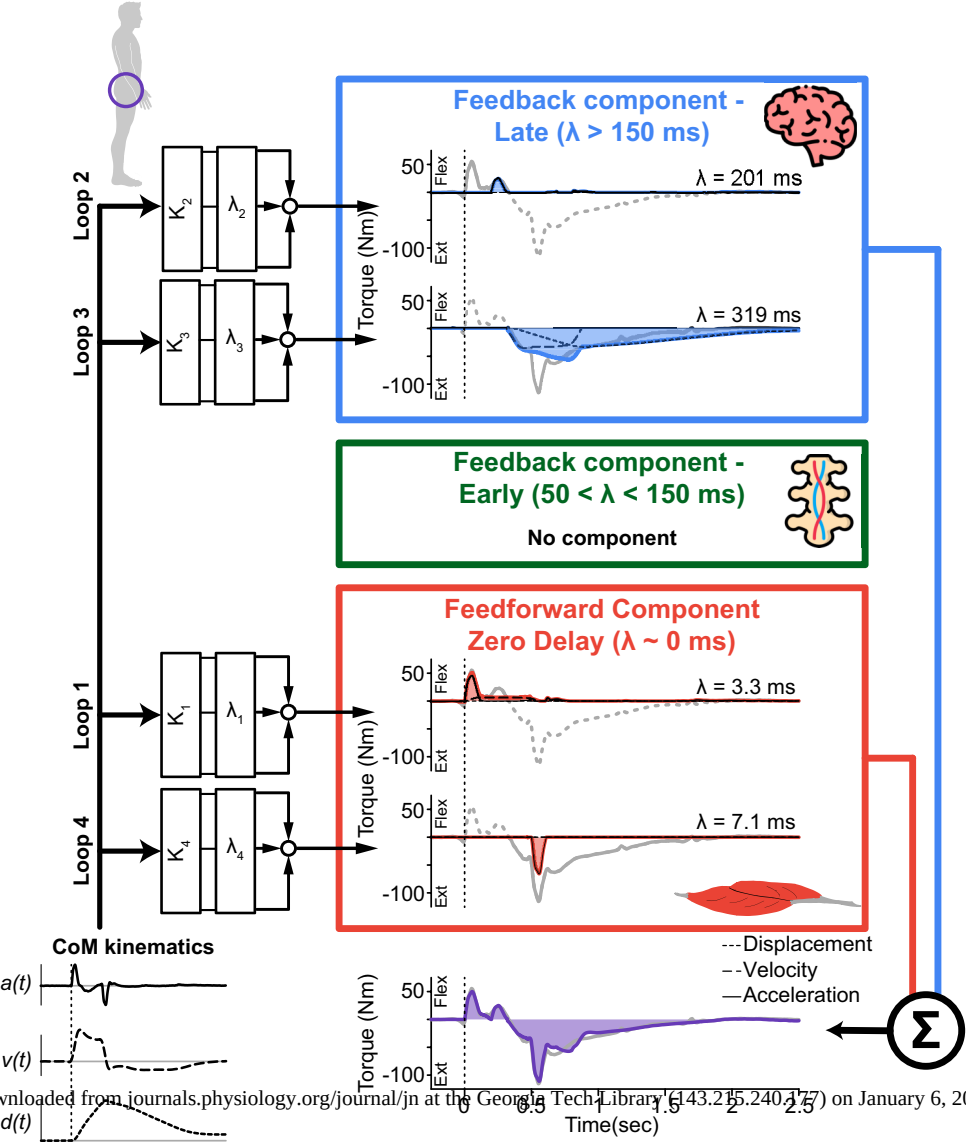

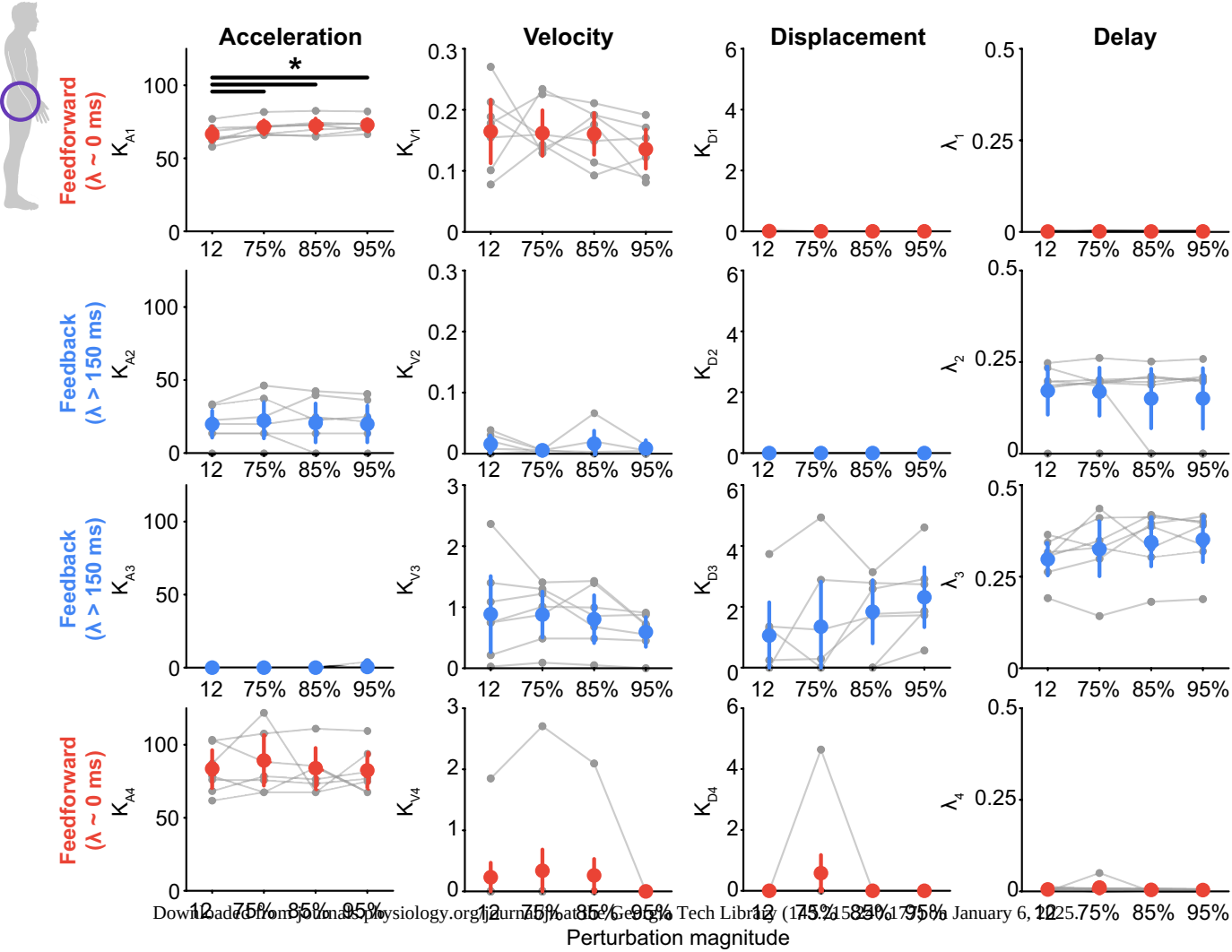

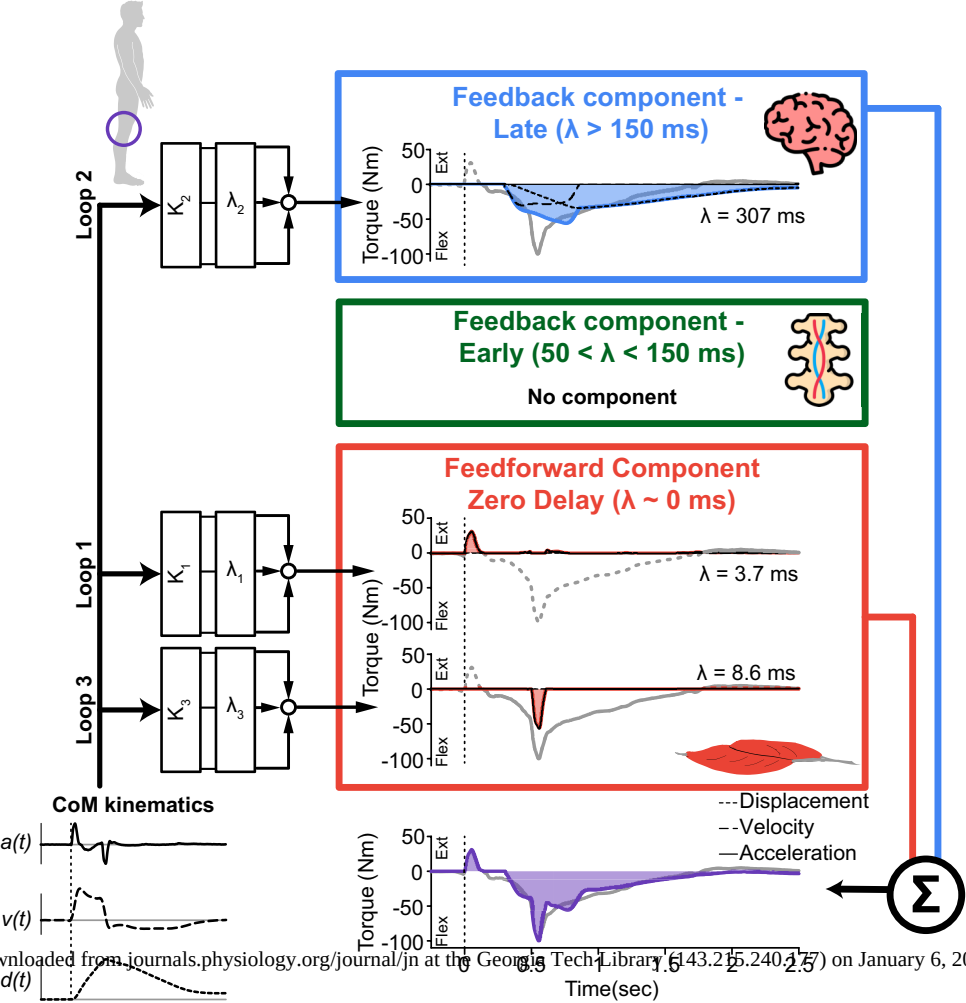

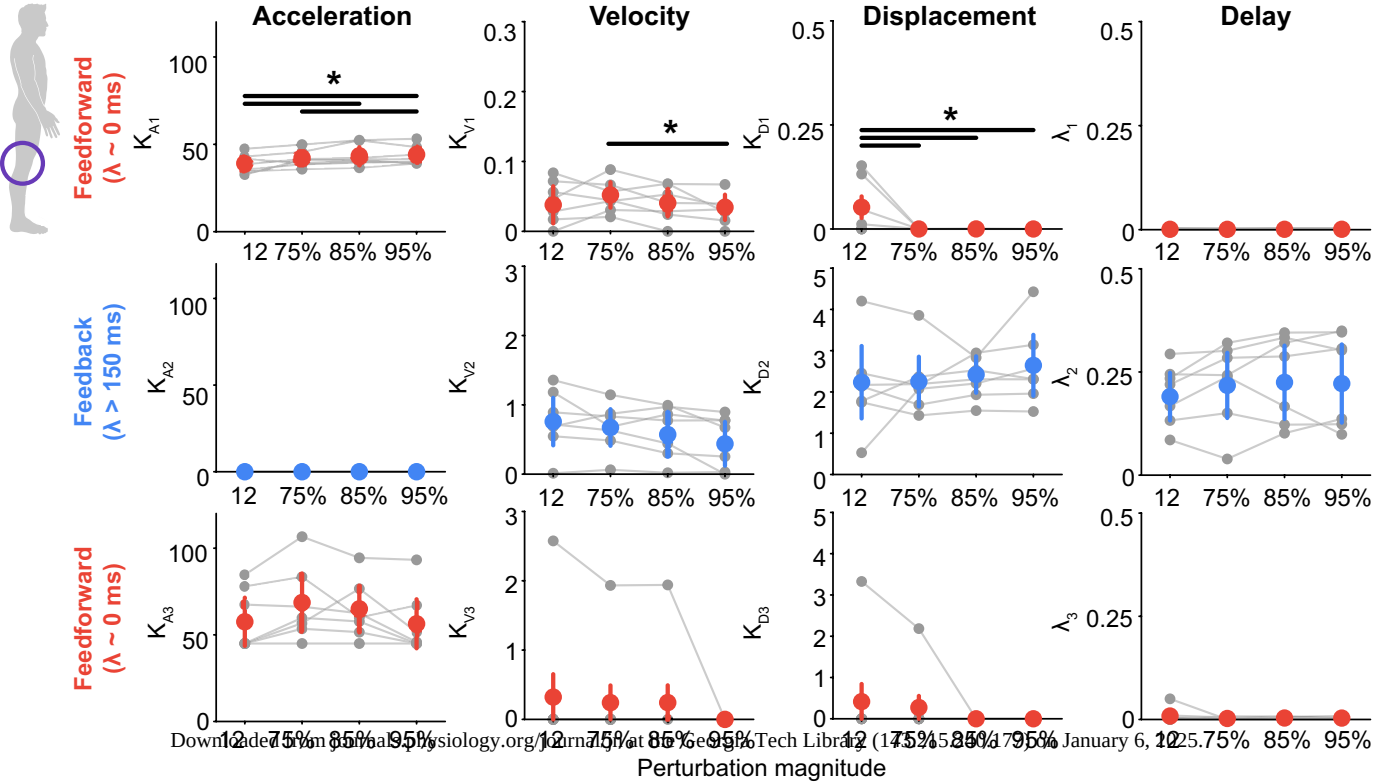

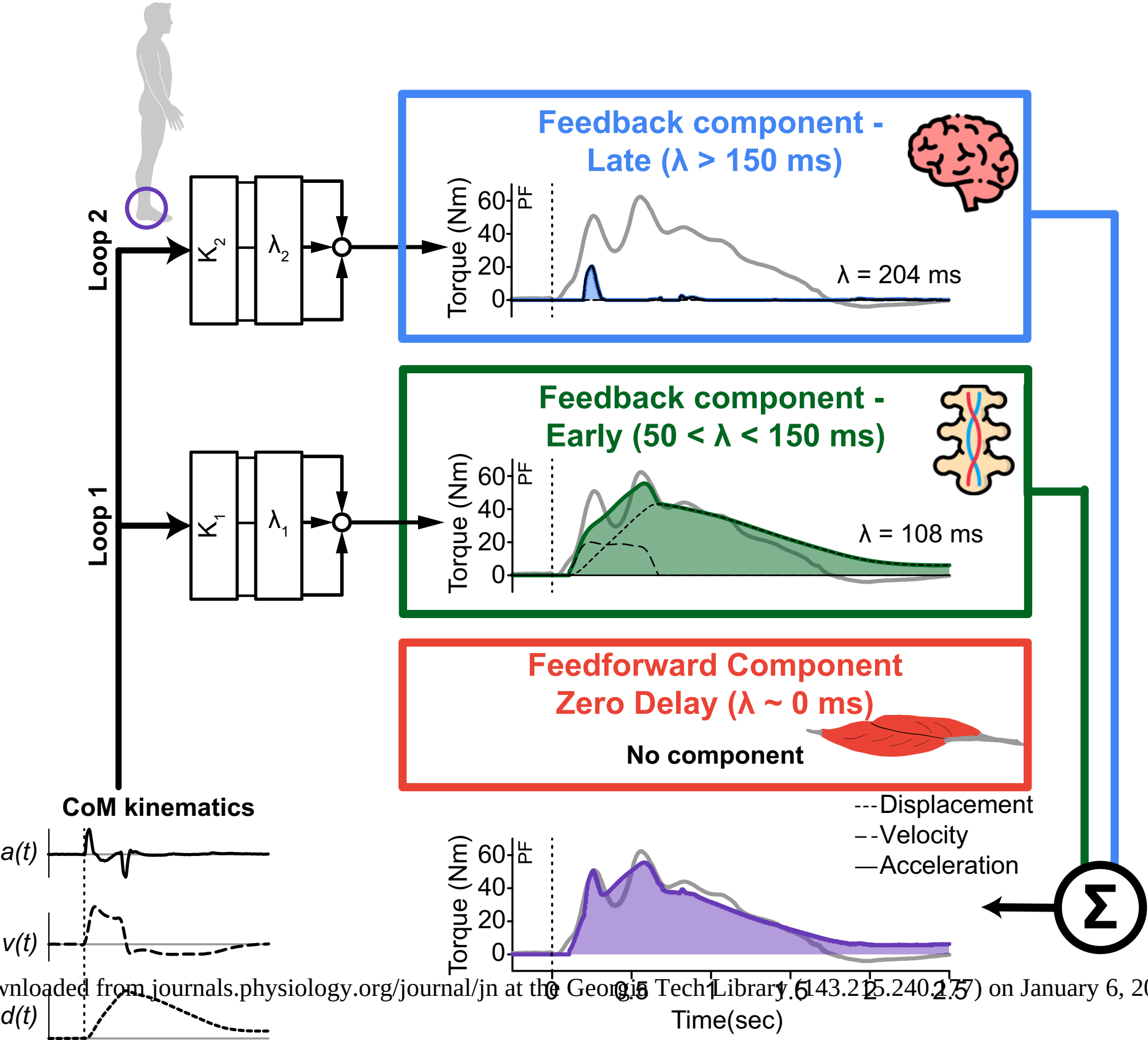

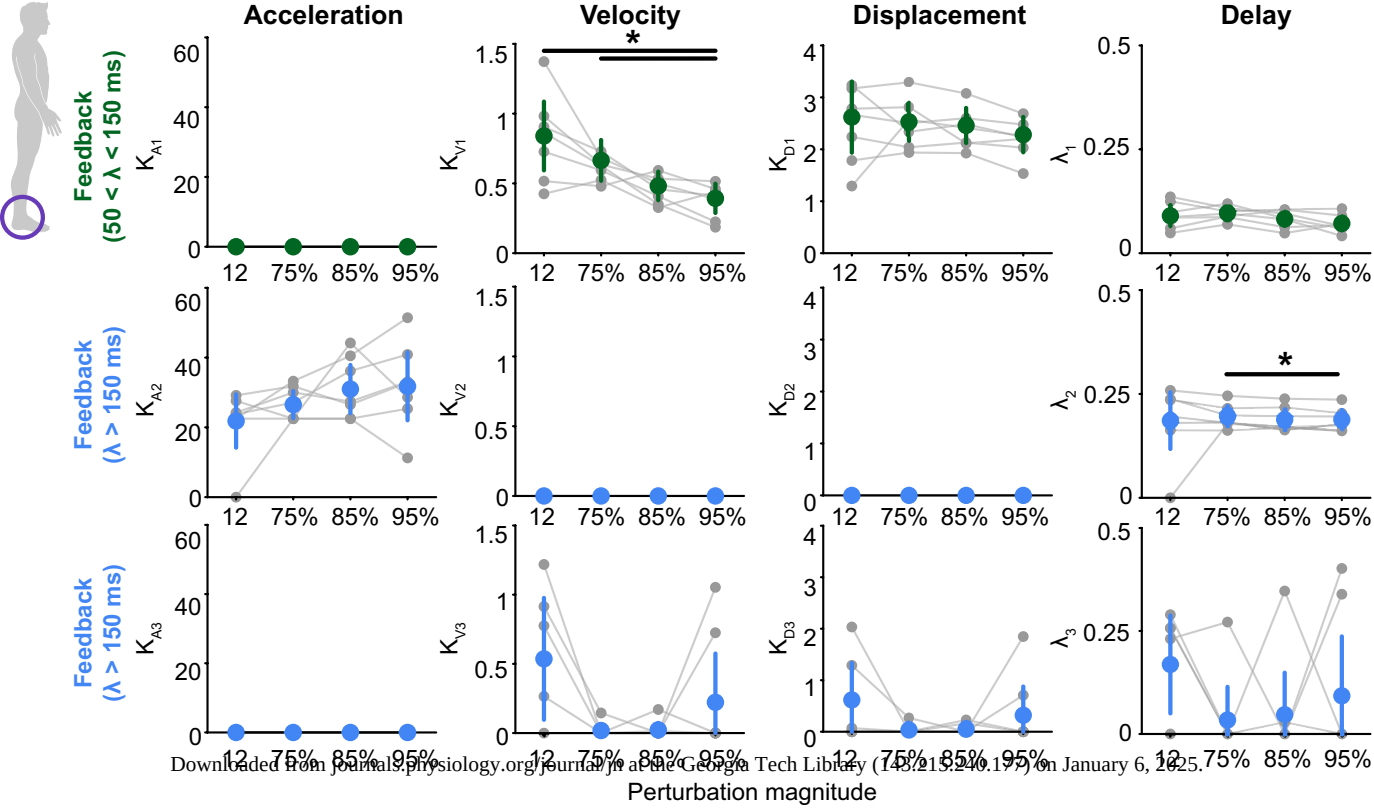

Using a sensorimotor response model (SRM), we decomposed reactive joint torques into feedforward and feedback contributions finding that the contribution from each pathway differed across joints